 doi:10.20944/preprints202009.0077.v1

Article

High performance zinc oxide nanorod-doped ion imprinted polypyrrole for the selective electrosensing of mercury II ions

Zouhair Ait-Touchente[1,*], Houssem Eddine El Yamine Sakhraoui[2], Najla Fourati[3,*], Chouki Zerrouki[3], Naima Maouche[2], Nourdin Yaakoubi[4], Rachid Touzani[1], Mohamed M. Chehimi[5,*]

[1] LCAE-FSO, Université Mohammed Premier, Oujda, 60000, Morocco ; r.touzani@ump.ac.ma (R.T.)
[2] Laboratoire d'Electrochimie et Matériaux, Université Ferhat Abbas, Sétif -1, 19000, Algeria ; h_sakhraoui@hotmail.com (H.E.E.Y.S.) ; nmaouche@univ-setif.dz (N.M.)
[3] SATIE, UMR CNRS 8029, Cnam, 75003 Paris, France ; fourati@cnam.fr (N.F.) ; zerrouki@cnam.fr (C.Z.)
[4] LAUM, UMR CNRS 6613, Le Mans Université, 72085, Le Mans, France ; nourdin.yaakoubi@univ-lemans.fr (N.Y.)
[5] ICMPE, UMR CNRS 7182, CNRS, 94320 Thiais, France ; chehimi@icmpe.cnrs.fr (M.M.C)
* Correspondence: chehimi@icmpe.cnrs.fr (M.M.C), zouhair.aittouchente@gmail.com (ZAT); fourati@cnam.fr (NF); Tel.: +33-6-63-05-46-08

Abstract: A biomimetic, ion-imprinted polymer (IIP) was prepared by electropolymerization of pyrrole at the surface of gold electrodes decorated with vertically grown ZnO nanorods. The vertical growth of the nanorods was achieved via an ultrathin aryl monolayer grafted by reduction of diazonium salt precursor. Pyrrole was polymerized in the presence of L-cysteine as chelatant agent and Hg(II) (template). Hg(II)-imprinted polypyrrole (PPy) was also prepared on bare gold electrode in order to compare the two methods of sensor design (Au-ZnO-IIP vs Au-IIP). Non-imprinted PPy was prepared in the same conditions, however in the absence of any Hg^{2+} template. The strategy combining diazonium salt modification and ZnO nanorod decoration of gold electrodes permitted to increase considerably the specific surface and thus to improve the sensor performances. The limit of detection (LOD) of the designed sensor was ~1 pM, the lowest value ever reported in literature. The dissociation constants between PPy and Hg^{2+} were estimated at [K_{d1} = (7.89 ± 3.63) mM and K_{d2} = (38.10 ± 9.22) pM]. The sensitivity of the designed sensor was found to be 0.692 ± 0.034 µA/pM. The Au-ZnO-IIP was found to be highly selective towards Hg(II) compared to cadmium, lead and copper ions. This sensor design strategy could open up new horizons in monitoring toxic heavy metal ions in water and therefore contribute to enhance environmental quality.

Keywords: Ionic imprinted polypyrrole; zinc oxide nanorods; mercury ions; diazonium salts; electrochemical sensor.

1.Introduction

One of the most serious problems affecting water is chemical pollution by organic or inorganic compounds such as pesticides and heavy metals, respectively. Among the inorganic pollutants, mercury (II) presents several health and ecosystem concerns [1–4]. Mercury gets released into the environment in large quantity through waste from thermal power plants, cement kilns, chlor-alkali plants, gold mining and trash incinerators (hazardous waste, medical waste, regular garbage, etc.) [5–8]. Exposure to mercury ions, even at low doses, can lead to severe central nervous system problems and vital human organs damage [2,8–11]. The discharge of mercury in the environment is forbidden by the United States Environmental Protection Agency (USEPA), European Union (EU) and World Health Organization (WHO). The environmental monitoring of mercury is very much important to avoid any further damage to the ecosystem [12]. The WHO has set a maximum

permissible limit of (1 μg.L^{-1}/5 nM) for mercury [13]. Developing reliable, sensitive and selective methods for the determination of mercury concentrations in food and drinking water is thus of particular significance.

Electrochemical sensors [4,14–17] are an excellent alternative combining miniaturization, speed and low cost. Field analysis of metal pollutants (even within a processing plant, for example) will be possible thanks to portable, wireless and ultra-sensitive potentiostats [18].

Ion imprinted polymers (IIPs) constitute a new class of sorbents possessing selectivity and affinity for separation or preconcentration or removal of target ions [14,16,19–21]. IIPs are prepared by formation of specific recognition sites in the framework of organic polymers and usually prepared by bulk polymerization method [16,22]. Template ions are then removed leaving cavities or "artificial receptor sites", in the polymer layer, that have appropriate shape, size and orientation of the functional groups for ion recognition at the rebinding stage [23–25]. For this reason, imprinted polymers are coined "plastic antibodies" for their ability to mimic antibodies. One of the most common applications of IIPs is solid phase extraction (SPE) which permits preconcentration of metal ions traces in environmental samples like natural water or seawater [26–28]. The IIPs as electrochemical sensors have shown remarkable selectivity, good thermal stability, low cost and excellent sensitivity [29–34].

The current challenge for most scientific researchers is to improve the performance of electrochemical sensors, including the limit of detection, in order to detect heavy metal ions at trace levels and by using very simple and inexpensive methods. To address this issue, we reasoned to increase the electroactive surface using nanoparticles to form a nanostructured sensing layer [35].

ZnO is one of the most used materials in applied sciences in recent years. It is a semiconductor; its wurtzite structure has a wide band gap (Eg=3.37 eV at 300 K) and a large exciton binding energy (60 meV) [36,37]. It is widely used for numerous applications such as laser diodes and gas sensors [38,39]. Synthesis and growth of ZnO at low temperatures [40,41] could be achieved by a plethora of techniques. To have a vertical and homogeneous growth of the ZnO nanorods, one can use the diazonium salts the derived aryl monolayer of which facilitates vertical growth. It is to note that without any diazonium surface modification the growth of ZnO nanorods is random [39].

In a recent conference proceeding [42], we have proposed to combine the advantage of diazonium surface modification for the vertical growth of ZnO nanorods and sensing properties of polypyrrole. In this follow-up, we provide an in depth study targeting to achieve ultimate detection limit using ZnO nanorod-embedded ion imprinted polypyrrole. Besides the central role of diazonium modification of the working electrode for the the growth of vertically aligned ZnO nanorods, such surface chemistry ensures robust adhesion of the polypyrrole sensing layer [43]. This strategy gathering the salient features of diazonium salts, ZnO nanorods and ion imprinting of polypyrrole has never been reported before at the exception of our short proceeding paper. We do believe it has much to offer to the surface scientist in a quest of making robust electrochemical sensor to address environmental issues.

Herein, a polypyrrole-based IIP was prepared in the presence of Hg(II) as a template and L-cysteine as a chelatant agent deposited on a gold electrode sequentially functionalized with diazonium salts and nanostructured with ZnO nanorods in order to have a very high roughness for the selective removal of mercury ions in a sample medium (KCl solution). For comparison, an IIP on a bare gold electrode was prepared. A non-imprinted polymer was also prepared in the same conditions of IIP but in the absence of any Hg(II). Electropolymerization time, incubation time, and number of cycles of electroreduction of diazonium salts were investigated and optimized. Electrode sensing materials were characterized by AFM in order to account for the morphological structures of the nanocomposites. Square wave voltammetry (SWV) experiments permitted to determine the optimal parameters for sensing Hg(II), namely linear response range, and the limit of detection of the ZnO-IIP sensor. Selectivity and competition between mercury and other ions was investigated

 doi:10.20944/preprints202009.0077.v1

by examining the electrochemical responses in the presence of copper, lead and cadmium taken as interfering metal ions.

2.Materials and Methods

2.1.Reagents

4-Aminobenzoic acid (≈ 99%), methanol (MeOH), H_2SO_4 (95%), H_2O_2 (30%), tetrabutylammonium tetrafluoroborate (99%), zinc acetate dihydrate (99.99%), sodium hydroxide (≈ 97%), hexamethylenetetramine (99%), acetonitrile (99.8%), potassium hexacyanoferrate(III) (≈ 99%), potassium hexacyanoferrate(II) trihydrate (≈ 98.5 %), potassium chloride, pyrrole (Py) (98%), lead nitrate $Pb(NO_3)_2$, copper(II) nitrate hemi(pentahydrate) (98%), and mercury(II) chloride (≈ 98%) were purchased from Sigma-Aldrich (Saint-Quentin-Fallavier, France). Pyrrole was purified through alumina basic column, then stored in dark at 4 °C. Cadmium sulfate 8/3-hydrate (≈ 99%) was supplied by VWR Prolabo (Fontenay-sous-Bois, France).

Zinc nitrate hexahydrate (≈ 99%) was obtained from Merck (Fontenay-sous-Bois, France), isopentyl nitrite (≈ 97%) was supplied by Alfa Aesar (Heysham, UK). The organic solvents used were of analytical grade and all aqueous solutions were prepared using ultrapure milli-Q water.

2.2.Instruments and characterization

All electrochemical measurements were carried out with a Bio-Logic portable potentiostat (model PG581). Conventional three-electrodes cell was used. A silver chloride electrode (SSC, +0.222 V vs. SHE), a platinum grid, and a gold substrate were the reference, counter and working electrodes, respectively.

Topographical characterization was performed by atomic force microscopy (AFM, MFP-3 Asylum Research). X-Ray photoelectron spectroscopy (XPS) analyses were conducted using a K Alpha apparatus (Thermo Fisher Scientific, East Grinsted, UK) fitted with an Al monochromatic X-ray source (1486.6 eV; spot size= 400 µm). A flood gun was used for charge compensation.

2.3. Surface functionalization with diazonium salt

Gold electrodes were first cleaned and activated by a drop of a piranha solution (98% H_2SO_4/30% H_2O_2 2:1 V/V) during 20 min. The surface modification of bare gold electrodes was carried out by 4-carboxybenzenediazonium tetrafluoroborate; this salt was *in situ* generated using 4-aminobenzoic acid [44] and was characterized by FTIR and carbon-13 NMR. Electro-reduction of diazonium salt on gold electrodes was performed by cyclic voltammetry at a scanning rate of 100 mV/s between -1.0 and 0.0 V/SSC for 20 cycles in a solution of acetonitrile containing 1 mM of diazonium salt and 0.1 M of tetrabutylammonium tetrafluoroborate. The modified electrodes were then rinsed with ultrapure water, ethanol and dried. The number of cycles has been optimized and controlled using ferrocyanide redox probe.

2.4. Synthesis, deposition and vertical growth of ZnO

A two-step process has been followed to grow the ZnO nanorods from ZnO seed particles in this low temperature method (Pacholski et al. [40]; Chander and Raychaudhuri [41]). In the first step, we have synthesized ZnO nanoparticles in order to use them as a seed layer on a diazonium-modified gold substrate for the second step consisting in the growth of ZnO nanorods.

 doi:10.20944/preprints202009.0077.v1

ZnO nanoparticles were prepared in methanol with 0.1 M of zinc acetate and 0.03 M of NaOH that were mixed under constant stirring and heating at 60 °C for one hour. The synthesized nanoparticles were then deposited by spin coating on the gold electrodes modified using the diazonium salt. The seeded substrates were heat-treated for 1 h at 125 °C for the sake of adhesion of the seed particles to the substrate.

The gold electrodes with the ZnO nanoparticles were placed upside down inside a beaker containing an aqueous solution of 30 mM zinc nitrate hexahydrate and 30 mM hexamethylenetetramine (HMT) solution in water kept at 95 °C for 5 hours with constant agitation. After desired time of growth, the samples were taken out of the solution, rinsed with ultra-pure water and dried in an oven preset at 125 °C for 1 hour.

2.5. Preparation of Au-IIP, Au-ZnO-IIP and Au-ZnO-NIP

Two different IIPs were prepared. the first one was made on a bare gold electrode and the second one was prepared on a gold electrode modified with diazonium salt and ZnO nanorods. These two configurations were carried out in two steps; the first in 2 seconds in a KCl solution containing 10^{-2} M of purified pyrrole (monomer) and 10^{-4} M of L-cysteine, the second step in 8 seconds in a KCl solution containing 10^{-2} M of purified pyrrole, 10^{-4} M of L-cysteine and 10^{-3} M of Hg(II) (template). These different steps were done by chronoamperometry at an applied potential of 1.05 V (vs Ag/AgCl). The non-imprinted polymer (Au-ZnO-NIP) was also prepared under the same conditions in the absence of any Hg^{2+} ion template.

2.6. Electrochemical measurements

The comparison between the prepared configurations, the Hg(II) detection tests, selectivity, competition between Hg(II) and other ions were controlled by square wave voltammetry between -0.95 and 0.95 V. under the following conditions : E-pulse: 0.01 V, E-step : 0.01 V, frequency : 25 Hz, equilibration time : 2 s). After each use, the IIP is extracted 20 min in EDTA and then 10 min in ultra-pure water with gentle stirring. Once the IIP is extracted it can be used another time.

3.Results and Discussion

3.1. Surface functionalization by 4-carboxybenzenediazonium tetrafluoroborate and quasi-vertical growth of ZnO

Scheme 1 displays the general three-step design of IIPs. To do so, we functionalized the surface of the gold electrode with carboxyphenyl groups from the corresponding diazonium salt (Scheme 1A, (1)) and then deposited (by spin coating) ZnO nanoparticles for the vertical growth of the ZnO nanorods (Scheme 1A, (2)). The second step consists in the formation of ion-imprinted polypyrrole by electropolymerization of pyrrole in the presence of L-cysteine (chelator) and Hg(II) template (Scheme 1(B)).

The different steps followed for the formation of ionic cavities are illustrated in the scheme 1C [45]. Removal of the template by washing, adapted to the nature of the functional monomer-template bond, leaves artificial sites capable of selective rebinding of the template.

Preprints (www.preprints.org) | NOT PEER-REVIEWED | Posted: 4 September 2020 doi:10.20944/preprints202009.0077.v1

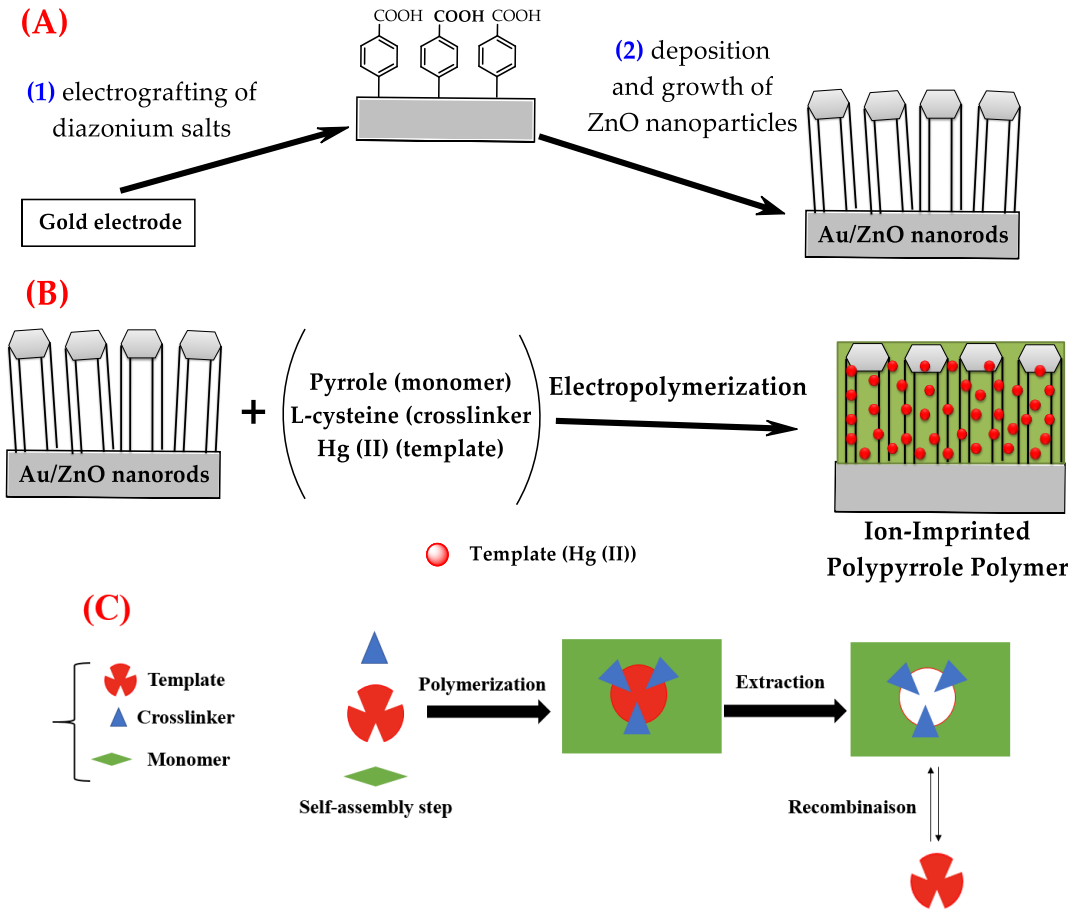

Scheme 1. Schematic illustration of experimental procedures. (**A**): Design of ZnO nanorods, (**B**) : design of the ion impritend polymer and (**C**) : principle of formation of an artificial receptor within a polymer matrix for hosting metal ion template at the rebinding step.

The electroreduction of the diazonium salt carried out by cyclic voltammetry in 20 cycles in the range -1.0 to 0.0 V (vs Ag/AgCl) gave a virtually zero reduction current (Figure 1(A)) resulting from a passivation of the electrode following the grafting of diazonium groups (formation of gold-diazo covalent bonds). The electroreduction peak is centered at -0.2 V (vs Ag/AgCl).

Passivation of the electrode was followed by cyclic voltammetry in presence of 0.01 M of $K_3[Fe(CN)_6]$ and 0.01 M of $K_4[Fe(CN)_6]$. Results presented in (Figure 1(B) indicate that the electrode was passivated while keeping its conductive character (Figure 1(B). red). The diazonium salt step makes it possible to have an almost homogeneous distribution of quasi-vertical growth of ZnO nanorods [39].

Preprints (www.preprints.org) | NOT PEER-REVIEWED | Posted: 4 September 2020 doi:10.20944/preprints202009.0077.v1

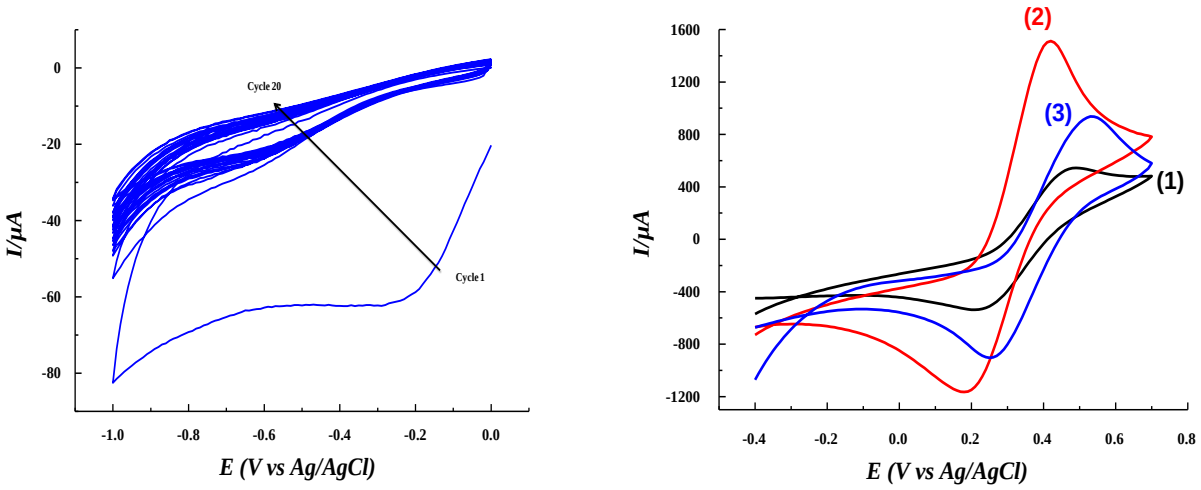

(**A**) (**B**)

Figure 1. Cyclic voltammograms corresponding to the electrografting of 4-carboxybenzenediazonium tetrafluoroborate. (**A**) Electroreduction, (**B**) Passivation test in H_2O/KCl 0.1 M solution, containing 0.01 M of $K_3[Fe(CN)_6]$ and 0.01 M of $K_4[Fe(CN)_6]$: (**1**) : as-received gold electrode ; (**2**) : cleaned electrode and (**3**) : after electrografting of the diazonium salt. Scan rate : 100 mV/s, 20 cycles for electrografting.

3.2. Preparation of IIPand NIP-based electrodes

Mercury oxidation voltammograms on gold electrodes yields two peaks; the first peak is attributed to the oxidation reaction Hg(0) to Hg_2^{2+} while the second peak is due to the transformation of Hg_2^{2+} into Hg(II) [46–48].

Before preparing the films on gold electrodes, we first characterized the signature of mercury with a gold disk working electrode in a solution containing mercury and KCl 0.1 M. The response obtained by SWV shows that the oxidation of mercury on gold gives two peaks at 0.061 and 0.71 V (vs Ag/AgCl) (Figure 2). The position of the two peaks depends on the pH of the solution, the nature of the working electrode, the electrolyte and the layer or film deposited on gold. In the following, we will consider the most intense peak located at 0.71 V (vs Ag/AgCl) which corresponds to Hg^{2+}. This dominant peak means that most of the mercury is converted to Hg^{2+}.

Preprints (www.preprints.org) | NOT PEER-REVIEWED | Posted: 4 September 2020 doi:10.20944/preprints202009.0077.v1

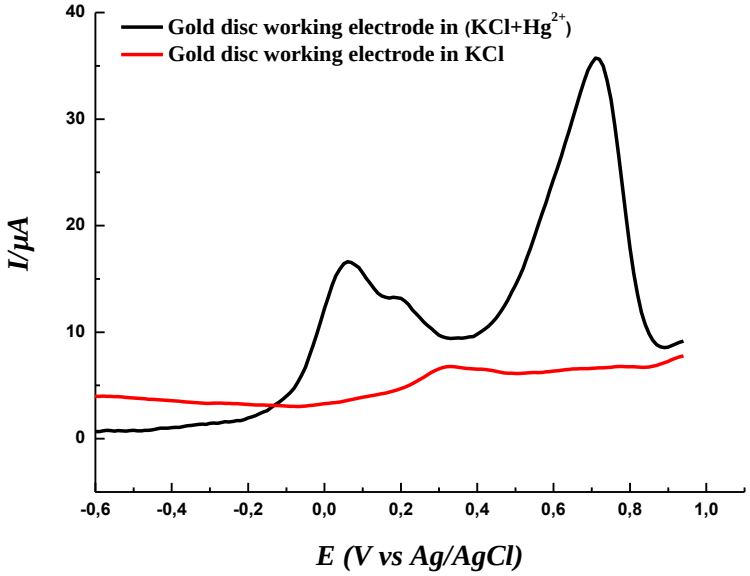

Figure 2. Characteristic peaks of mercury oxidation on gold electrode in H_2O/KCl 0.1 M solution. Conditions : E-pulse : 0.01 V, E-step : 0.01 V, frequency : 25 Hz, equilibration time : 2 sec.

Both ZnO-IIP and ZnO-NIP were prepared by chronoamperometry (Figure 3(A)), then compared using square wave voltammetry (SWV) (Figure 3(B)). On the one hand, one can notice the obvious difference between the responses of ZnO-IIP and ZnO-NIP; *i.e.* mainly for the peak current corresponding to potential around 0.62 V (vs Ag/AgCl) in the case of ZnO-IIP will be considered for quantitative monitoring of mercury. On the other hand, the removal of Hg^{2+} from ZnO-IIP by EDTA leads to flat SWV response, close to that of ZnO-NIP (Figure 3(B)). This means that all receptor sites have been released and thus can be reused for rebinding the target ions.

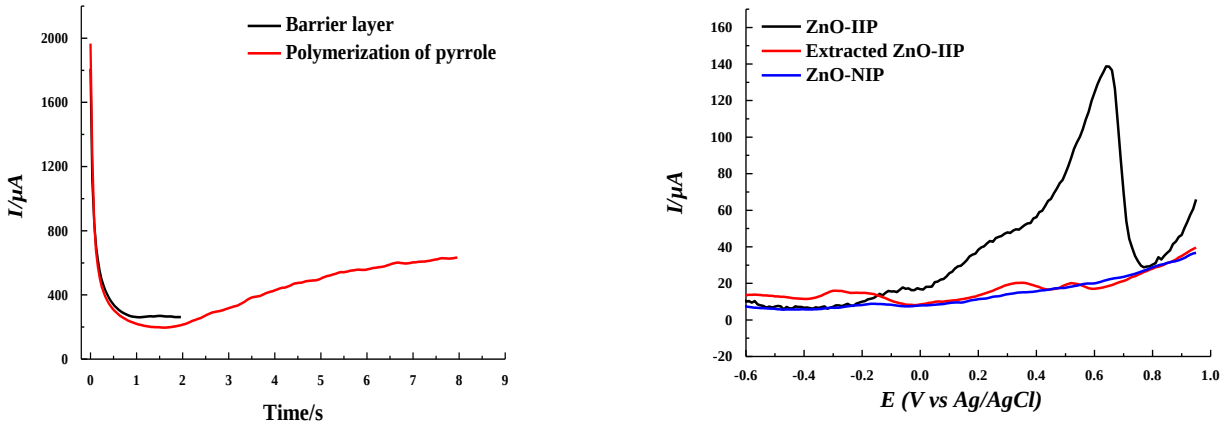

(A) (B)

Figure 3. (A) : Electropolymerization of pyrrole by chronoamperometry at a constant potential of 1.05 V/SSC. (black) Barrier layer, (red) Polymerization of pyrrole in the presence of L-cysteine and Hg^{2+} (B) : SWV of IIP and NIP in H_2O/KCl 0.1 M solution.

In order to showcase the central role of ZnO nanorods, we have prepared two different IIPs, the first one was prepared directly on bare gold electrode and the second IIP was prepared on Au-ZnO. After extraction of the metal ions from these two IIPs in EDTA solution, they were incubated in 10^{-3} M mercury solution for 20 minutes for rebinding test.

Preprints (www.preprints.org) | NOT PEER-REVIEWED | Posted: 4 September 2020 doi:10.20944/preprints202009.0077.v1

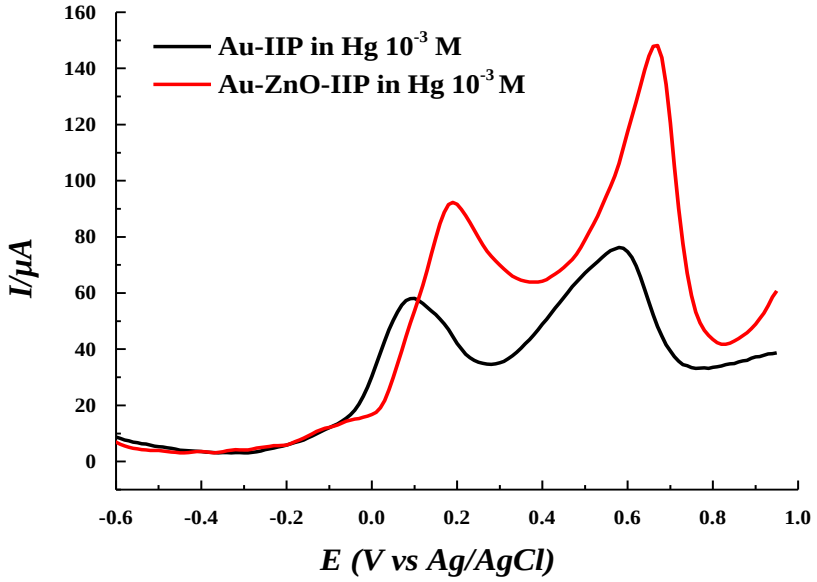

Figure 4. SWV voltammograms in H_2O/KCl 0.1 M solution after incubation of Au/Hg-IIP and Au-ZnO/Hg-IIP in 10^{-3} M Hg^{2+}. Conditions: E-pulse : 0.01 V, E-step : 0.01 V, frequency : 25 Hz, equilibration time : 2 sec.

Square wave voltammograms presented in Figure. 4 show that the current intensity of the IIP prepared on ZnO nanorods is twice higher than that prepared on flat gold elctrodes. This can be related to the increase of the specific surface, which makes it possible to deposit more IIP and thus a large number of artificial sites to capture more Hg^{2+} ions.

3.3. *Choice and role of the chelatant agent*

The formation of mercury receptor sites in the ZnO-IIP was done using L-cysteine, a chelator of mercury. This choice was driven by the thiophilicity of metal ions [48–50], and especially high affinity of L-Cys for Hg^{2+} [51]. L-cysteine is an ideal compound, bearing electron-rich functional groups sush as -NH_2, -COOH and -SH, which allow to have Hg-cysteine complex [52–54]. The incorporation of L-cysteine/Hg(II) into polypyrrole is likely to take place via electrostatic bonds between the carboxylic group of L-cys and the nitrogen of pyrrole (Scheme 2) [54].

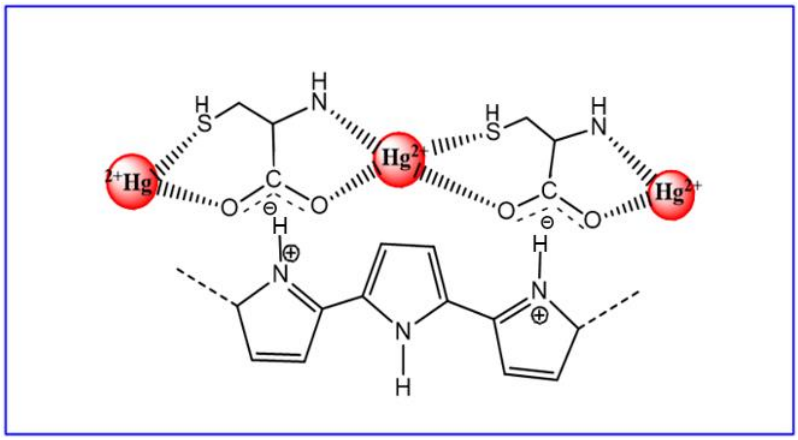

Scheme 2. Schematic representation of Hg(II) complexation by L-Cysteine in the polypyrrole layer.

Preprints (www.preprints.org) | NOT PEER-REVIEWED | Posted: 4 September 2020 doi:10.20944/preprints202009.0077.v1

3.4. *Surface analysis by XPS*

Figure 5 shows the survey spectra for the bare gold electrode, Au/diazo-COOH, Au-diazo-ZnO nanoparticles, Au-diazo-ZnO nanorods, ZnO-IIP, and ZnO-NIP.

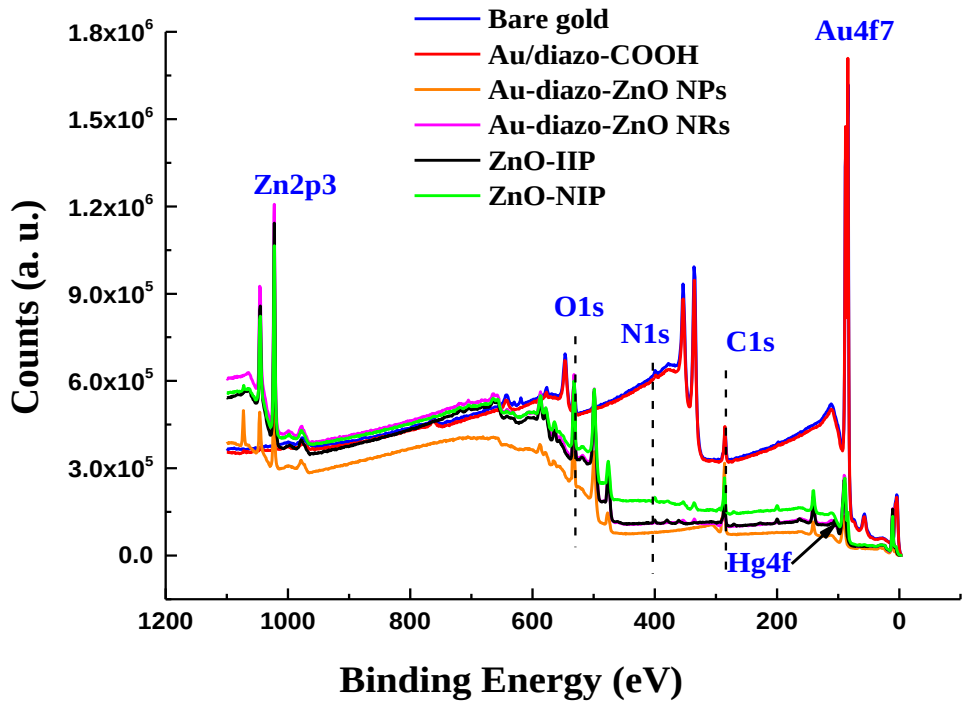

Figure 5. XPS survey scans of : Au electrode, Au/diazo-COOH, Au-diazo-ZnO nanoparticles, Au-diazo-ZnO nanorods, ZnO-IIP, and ZnO-NIP.

Firstly, comparison of the XPS spectrum of bare gold electrode with Au/diazo-COOH confirms the effective reductive electrografting reaction of the diazonium salt on the gold electrode. Indeed, it is noticed the presence of characteristic signals of the diazo-COOH, namely C1s and N1s peaks centred at 285 eV and 400 eV, respectively (Figure 5). It should be noted that the surface-grafted layer seems to be relatively thin (less than 10 nm), this has also been confirmed by the atomic percentages shown in Table 1. The atomic percentage of gold has decreased from 41.6% for the bare gold electrode to 35.8% after electrografting of the diazonium salt with a small increase in the percentage of carbon (grafting of the diazonium salt while keeping the conductive activity of the electrode).

Table 1. Surface chemical composition of Au electrode, Au/diazo-COOH, Au-diazo-ZnO nanoparticles, Au-diazo-ZnO nanorods, ZnO-IIP, and ZnO-NIP nanocomposites as determined by XPS.

Samples	Au	C	O	N	Zn	Hg
Bare gold electrode	41.6	42.2	16.2	-	-	-
Au/diazo-COOH	35.8	45.9	14.3	3.97	-	-
Au-diazo-ZnO NPs	-	60.6	28.3	0.43	10.7	-
Au-diazo-ZnO NRs	0.87	32.3	38.5	0.97	27.4	-
ZnO-IIP	0.07	43.0	33.2	2.38	20.7	0.57
ZnO-NIP	1.61	43.5	33.3	2.95	18.7	-

After the deposition of ZnO nanoparticles by spin-coating, we have the appearance of a peak at 1022 eV which corresponds to the $Zn2p_{3/2}$ of ZnO (Figure 5), with an atomic percentage of 10.7%. After the ZnO growth step, the atomic percentage of zinc and oxygen increase (27.4% and 38.5%

 doi:10.20944/preprints202009.0077.v1

respectively). We can also note a decrease in the peaks corresponding to the $Au4f_{7/2}$ and C1s signals (Figure 5), which confirms the success of the ZnO nanorods growth step.

Comparison of the XPS spectra of ZnO-IIP and ZnO-NIP (Figure 5) indicates the grafting of a polypyrrole film on the surface of the electrode. However, mercury is present only in the case of IIP material, which indicates that the template has been well trapped in the polymeric matrix. The atomic percentage of Zn for NIP and IIP decreased due to screening ZnO with polypyrrole (Table 1).

3.5. Topographical characterization

The atomic force microscopy (AFM) measurements have been carried out in order to monitor the topographic changes after each surface functionalization step. The evidence of nanorod growth is not the purpose herein, that being clearly shown in a previous work [55]. Therefore, we can use a standard tapping mode AFM probes instead of high aspect ratio ones. The robustness of the former allows comparative investigation of several samples surface, without changing the probe. 2D AFM images of (5×5) μm^2 have thus been achieved on the same sample, before (bare gold substrate) and after each functionalization step (diazonium salt, ZnO nanoparticles, ZnO nanorods, then IIP), and finally after extraction of Hg^{2+} template (Figure 6).

Preprints (www.preprints.org) | NOT PEER-REVIEWED | Posted: 4 September 2020 doi:10.20944/preprints202009.0077.v1

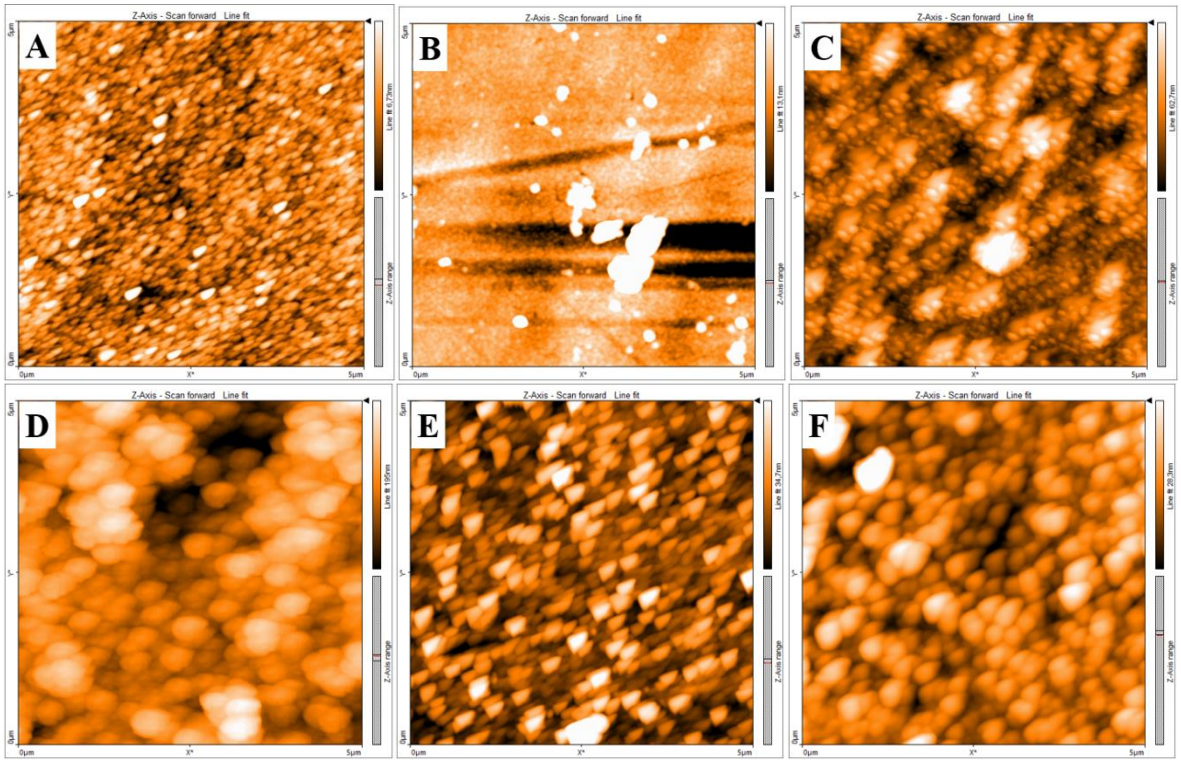

Figure 6. 5×5 µm² AFM images of (**A**) Bare gold electrode, (**B**) Gold electrode-diazonium salt, (**C**) Au/Diazo/ZnO nanoparticles, (**D**) Au/Diazo/ZnO nanorods, (**E**) Au/Diazo/ZnO NRs-IIP, (**F**) Extracted Au/Diazo/ZnO NRs-IIP.

The AFM images (Figs 6A to 6F) exhibit a granular-like aspect and seem different enough in both shape and size. The grafting of diazonium salt (image 6B) leads to the formation of a layer veiling the granular appearance. The latter is again visible (image 6C) after grafting the ZnO nanoparticles, with higher contrast than for bare gold surface (image 6A). Image 6D that corresponds to ZnO nanorods growth, exhibits the largest size of surface singularities, which seems reduced by the electropolymerization of IIP (image 6E). The extraction of template from IIP film (image 6F) leads to a different aspect that is probably due to the local rearrangement of the IIP.

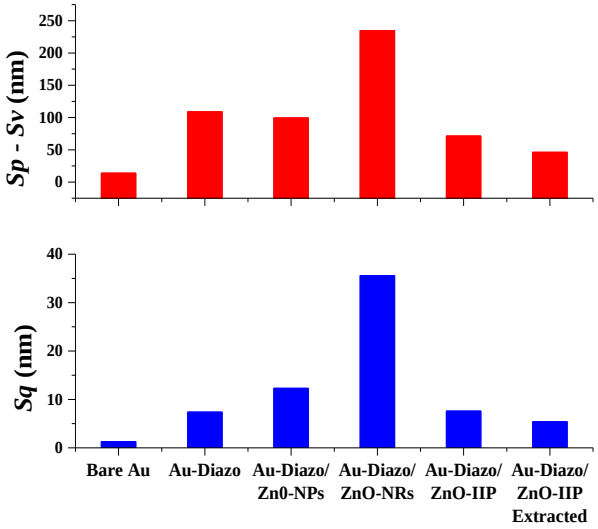

Figure 7. Root-mean-square height (Sq) and peak-valley height (Sp-Sv) values after the different functionalization steps, from bare gold substrate to electrosynthesis of IIP and the further extraction of the imprinted Hg^{2+} template ions.

Preprints (www.preprints.org) | NOT PEER-REVIEWED | Posted: 4 September 2020 doi:10.20944/preprints202009.0077.v1

Despite the usefulness of AFM images, the qualitative description remains limited due to the high contrast that may exist in the presence of multiple defects with high amplitudes. Measurements should therefore be considered from a quantitative point of view, by considering relevant roughness statistical parameters, such as rms roughness (*Sq*) and peak-valley height (*Sp-Sv*). Values of these two parameters are presented in Figure 7.

As expected, each surface modification leads to a noticeable change of roughness parameters. The most important one occurs after diazonium salts grafting. This first step of functionalization led to an increase of (*Sq*) and (*Sp-Sv*) parameter values by a factor of 5.7 and 7.8, respectively. The increase in roughness continued with the grafting of ZnO NPs, but to a lesser extent, by a factor of 1.7 for (*Sq*) while (*Sp-Sv*) value remains relatively stable. The growth of the nanorods generated a variation of the two considered parameters by a factor of 2.9 and 2.4, respectively. The electro-polymerization of IIP produced a coating effect resulting in a significant decrease in the values of the two roughness parameters by a factor of 4.7 for (*Sq*) and 3.3 for (*Sp-Sv*). These two parameters decreased by a factor of about 1.5 only, after the analyte extraction step. This slight decrease is probably due to the local rearrangements which occurs once the Hg^{2+} ions extracted from the polymer matrix.

3.6. Extraction time in EDTA and incubation time in mercury solutions

Ethylenedinitrilo tetraacetic acid (EDTA) has been used in this work to extract mercury ions from the ZnO-IIP sensor. EDTA is an acid that is difficult to biodegrade. It is a stable chelator used in several applications such as the medical field and the nuclear industry but it is also used to adsorb heavy ions through functional groups avoiding their precipitation *[56–58]*. Experiments (results not shown here) indicate that the optimum extraction was obtained by incubating the IIP in EDTA 0.1 M, during 20 min, and by rinsing after that the films for 10 minutes in ultra-pure water.

The film obtained after extraction was incubated in a mercury solution (10^{-4} M) at different periods of time. Results presented in Figure 8 indicate that the number of Hg(II) ions captured by the sensor increased only slightly between 20 and 40 min, compared to the sharp increase between 5 and 20 min of incubation. For practical reason, the incubation time was set to 20 min.

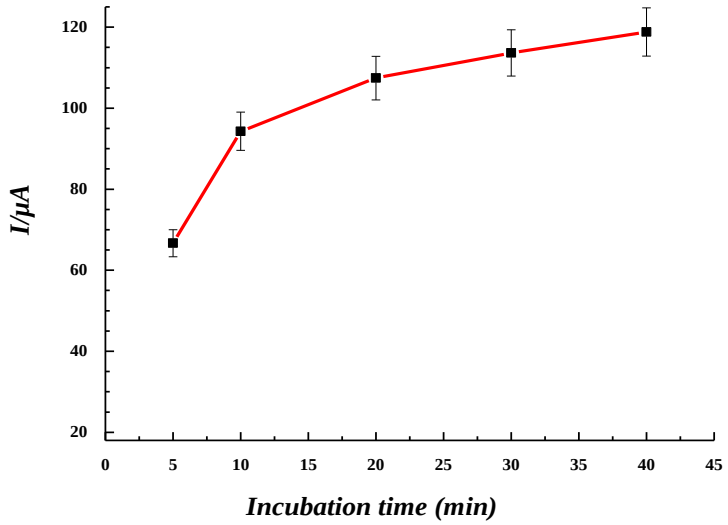

Figure 8. Hg-IIP response after different incubation times in 10^{-4} M mercury solution/H_2O/KCl 0.1 M.

3.7. Electrochemical sensing of mercury

SWV was used to investigate the electrochemical response of the ZnO/Hg(II)-IIP sensor towards mercury in solution at different concentrations. Sensor response has been recorded, via the characteristic peak current, for concentrations between 10^{-12} and 10^{-3} M (Figure 9).

The sensor limit of detection (LOD) was determined from the lowest concentration that gave a visible signal, instead of from the signal to noise ratio of 3 as usually done. Here, the obtained LOD of 1 pM is way lower than the WHO maximum permissible limit in drinking water of (1 µg/L).

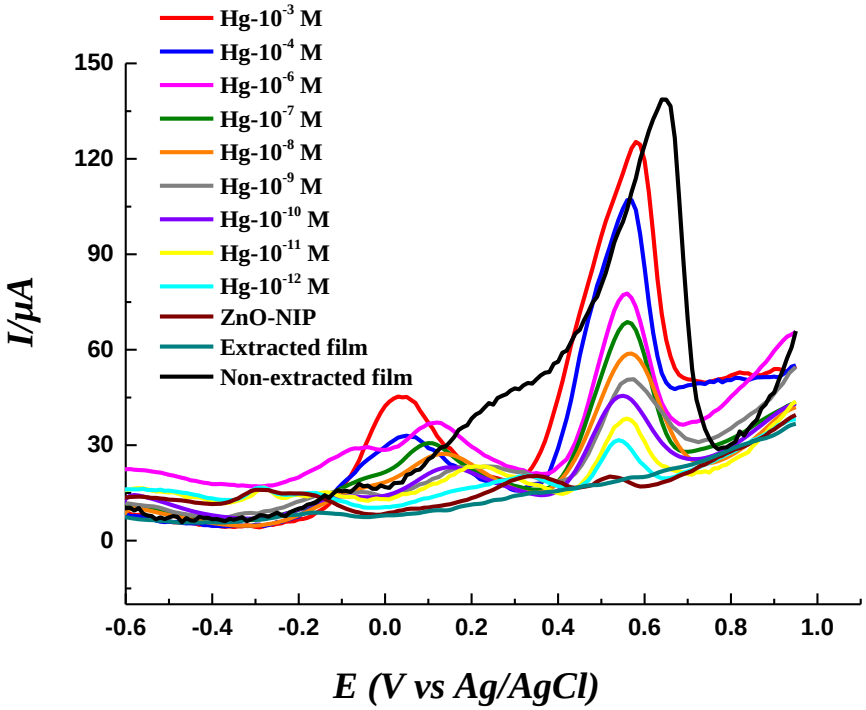

Figure 9. Follow up of pic currents variations (determined from SWV measurements in H_2O/KCl 0.1 M solution) according to the potential. Conditions: E-pulse: 0.01 V, E-step: 0.01 V, frequency: 25 Hz, equilibration time: 2 sec.

To confirm the performance of the sensor, this Hg(II) detection step was done on three different ZnO/Hg(II)-IIP, the average calibration curve is shown in Figure 10 (variations of output signal of electrochemical IIP-based sensor versus Hg(II) concentrations).

Preprints (www.preprints.org) | NOT PEER-REVIEWED | Posted: 4 September 2020 doi:10.20944/preprints202009.0077.v1

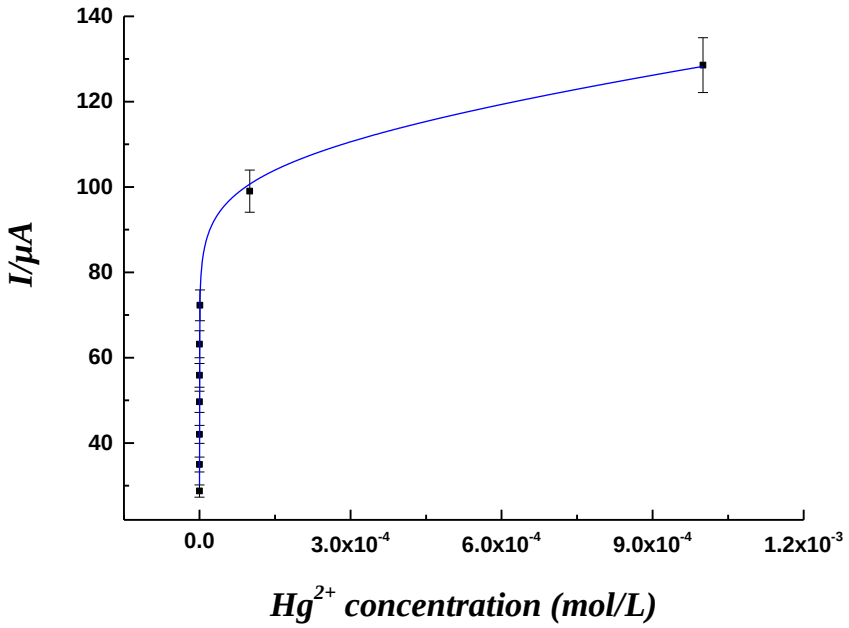

Figure 10. Peak current variation versus Hg(II) concentration; electrochemical experimental data were fitted by a combined model (one binding site + Hill model).

The dissociation constant K_d is an important parameter that determines the degree of affinity between the polymer and the template. Different analytical models were tested to fit the experimental data of the electrochemical measurements. The most appropriate one was combination between one site model and Hill model (Figure 10). The choice of this model makes it possible to take into consideration the mechanical restructuring of polymers at the nanometric scale [59].

$$Y(C) = \frac{A_1 \times C}{K_{d1} + C} + \frac{A_2 \times C^{\propto}}{K_{d2} + C^{\propto}}$$

where y (C) is the output sensor's signal response (current) for a given concentration (C) of Hg(II). K_{d1}, and K_{d2} are the first and second dissociation constants, A_1 and A_2 are empiric constants, and α is an empiric ponderation exponent. The values obtained for K_{d1} and K_{d2} were of order of (7.9 ± 3.6) mM and (38.1 ± 9.2) pM], respectively. The value of K_{d2} is consistent with that linked to the binding of Hg(II) to the Cys4 site in CP-CCCC peptide, which shows that the IIP can imitate biological entities in terms of affinity for heavy ions [51,59]. The α value of 0.06 ± 0.002, indicates positive cooperative interactions between Hg(II) ions and other binding sites [51].

The sensor sensitivity, computed from the slope at the origin of current/concentration curves (*i.e.* at lower concentrations), was of order of 0.692 ± 0.034 μA/pM. This value shows that this LCys-PPy sensor prepared on Au-ZnO to capture mercury is very sensitive compared to several sensors intended to detect heavy metals [60–62]. In addition to these interesting metrological features, we also tested the selectivity of the sensor by comparing the recognition of the targeted Hg(II) to lead, cadmium and copper ions. The rationale for this set of ions is the following: Cd^{2+} has an ionic radius close to that of Hg^{2+}; Cu^{2+} has a lower ionic radius than Hg^{2+} whereas Pb^{2+} is larger ion than the targeted Hg^{2+}.

Preprints (www.preprints.org) | NOT PEER-REVIEWED | Posted: 4 September 2020 doi:10.20944/preprints202009.0077.v1

We first incubated the extracted film in a solution containing an ion of the chosen ions with a concentration of 10^{-4} M (Figure 11(A)). The second step is to mix several ions with Hg^{2+} with the same concentration of each ion (Figure 11(B) black curve) and another test in a solution containing Pb^{2+} and Hg^{2+} with a concentration of Pb^{2+} greater than 100 times that of Hg^{2+} (Figure 11(B) red curve).

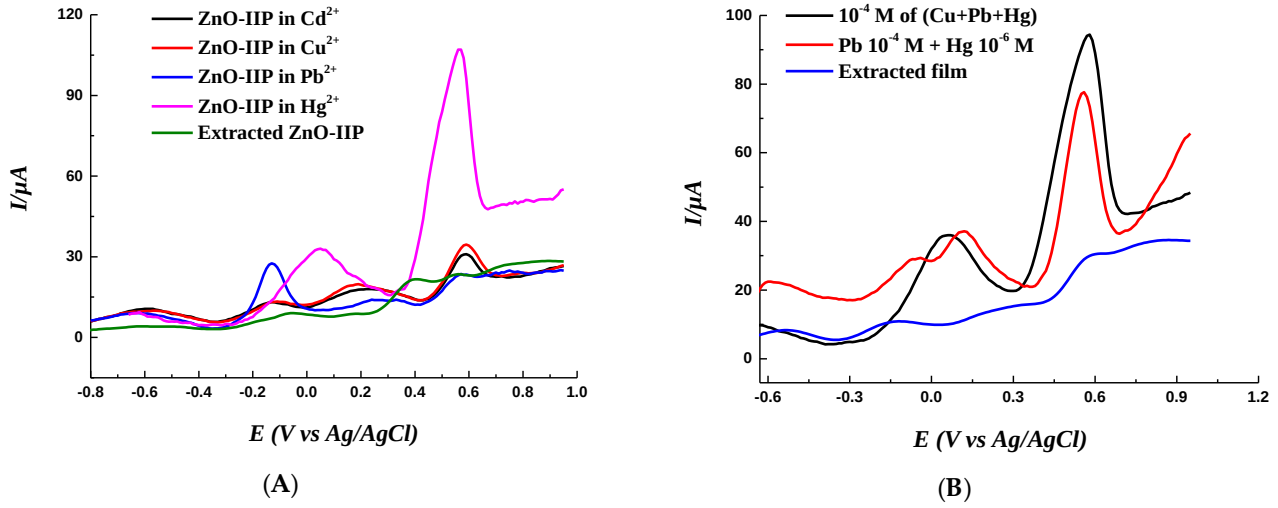

Figure 11. Evaluation of sensor's selectivity. (A) : SWV curves in H_2O/KCl 0.1 M solution of ZnO/Hg(II)-IIP electrodes incubated in 10^{-4} M solutions of either mercury, cadmium, lead or copper ions for 20 minutes. (B) : Competition tests. Conditions : E-pulse : 0.01 V, E-step : 0.01 V, frequency : 25 Hz, equilibration time : 2 sec.

The incubation of the extracted film each time in 10^{-4} M solution of a single chosen ion (Figure 11 (A)) shows that ZnO-IIP is specific for Hg(II).

The competition tests (Figure 11(B)) which are carried out by incubating the extracted film in a solution containing equal concentrations (10^{-4} M) of Cu^{2+}, Hg^{2+} and Pb^{2+} ions have shown that in the presence of mercury, the extracted film detects Hg^{2+} specifically.

In a mixture containing 10^{-4} M of Pb^{2+} and 10^{-6} M of Hg^{2+}, we note that despite the low concentration of mercury with the presence of other ions, the sensor remains specific to Hg(II), hence the importance to shape the receptor sites with this template. This also shows that there is no competitive chemisorption of Pb^{2+} which hampers the response of the sensor to the Hg^{2+} ions.

The performances of the IIP sensor designed so far are compared to those of a fistful of other sensors described in the literature (Table 2). Embedding ZnO nanorods in the IIP film provided unique LOD, as low as 1 pM.

Preprints (www.preprints.org) | NOT PEER-REVIEWED | Posted: 4 September 2020 doi:10.20944/preprints202009.0077.v1

Table 2. Comparison of the analytical performance of ZnO-IIP to those of other handpicked relevant sensors reported in the literature.

Electrode	Analytical Method	Electrolyte	LOD	Ref
Glassy carbon electrode GC/SH/AuNPs	Square Wave Anodic Stripping Voltammetry (SWASV)	HCl solution	10 nM	[13]
Carbon-paste electrode (CPE)	Differential pulse voltammetry (DPV)	HCl solution	0.52 nM	[31]
Glassy carbon electrode	Difference pulse voltammetry (DPV)	PBS (pH 7.0)	0.42 nM	[63]
Carbon-paste electrode (CPE)	Electrochemical Impedance Spectroscopy (EIS)	Nitrate solution	1.95 nM	[64]
Commercial screen-printed carbon electrode (SPCE)	Differential pulse voltammetry (DPV)	KNO_3/HNO_3 solution (pH 2.7)	0.104 nM	[65]
Glassy carbon electrode	Square wave anodic stripping voltammetry (SWASV)	$K_3[Fe(CN)_6]$ solution	0.1 nM	[66]
Carbon paste electrode (CPE)	Square wave anodic stripping voltammetry (SWASV)	HCl solution	18 pM	[67]
Glassy carbon electrode (GCE)	Differential pulse voltammetry (DPV)	PBS (pH 7.0)	0.2 µM	[68]
Carbon nanomaterials/AuNPs	Anodic stripping voltammetry (ASV)	KCl solution	0.03 µM	[69]
Zinc oxide nanorods grafted on a Gold electrode	**Square Wave Voltammetry (SWV)**	**KCl solution**	**1 pM**	**This work**

4. Conclusion

A new electrochemical sensor based on biomimetic ion-imprinted polymer for the detection of mercury (II) traces was prepared on a gold electrode with a strategy based on the combination of the surface modification with a diazonium salt and the growth of ZnO nanorods followed by electropolymerization of the pyrrole in the presence of the template (Hg^{2+}) and L-cysteine as crosslinker. These two steps (diazonium salt and ZnO nanorods) permitted to increase the performance of the final sensor (Au-diazo-ZnO/IIP) in terms of selectivity and limit of detection (LOD) which is in the picomolar range. This is proved by investigating the performances of an IIP prepared directly on a bare gold electrode, without any surface modification and in the absence of any ZnO nanorods.

The fit of the electrochemical results obtained by the one site/Hill model allowed us to determine the dissociation constants [K_{d1} = (7.89 ± 3.63) mM and K_{d2} = (38.10 ± 9.22) pM] as well as the sensitivity is equal to 0.692 ± 0.034 µA/pM.

The competitivity and selectivity tests were undertaken using several ions such as Cu^{2+}, Pb^{2+}, and Cd^{2+} taking into account the ionic radius and their concentration in an aqueous medium. IIP showed excellent ability to distinguish between mercury and different competitive ions even at low concentration. Au-diazo-ZnO/IIP can therefore be used for environmental applications to detect mercury in the laboratory or for field analysis using a portable potensiostat.

 doi:10.20944/preprints202009.0077.v1

Acknowledgements

The authors are indebted to SATIE and ICMPE for internal financing to support the project. N.Y wishes to thank La Région Pays de Loire for financial support through the LMAC/MEMSAW project, and H.E.E.Y.S is grateful to the Algerian Ministry of Higher Education and Scientific Research for the provision of PNE grant No 474.

Author Contributions

Conceptualization of the research work by Z.A.T., N.F., C.Z.
Methodology by Z.A.T., N.F., C.Z., M.M.C.
Validation by Z.A.T., N.F., C.Z., R.T., M.M.C.
Formal Analysis by Z.A.T., H.E.E.Y.S., N.F., C.Z., N.M., N.Y., M.M.C.
Writing of Original Draft was done by Z.A.T., N.F., C.Z., M.M.C.
Writing: Review and Editing by Z.A.T., H.E.E.Y.S., N.F., C.Z., N.M., N.Y., R.T., M.M.C.
Supervision: N.F., C.Z., R.T., M.M.C.
Funding Acquisition: N.F, C.Z., N.M., N.Y., R.T.

Conflict of interest

The authors declare no conflict of interest.

References

1. Pacyna, E.G.; Pacyna, J.M. Global Emission of Mercury from Anthropogenic Sources in 1995. **1995**, 17.
2. Tchounwou, P.B.; Ayensu, W.K.; Ninashvili, N.; Sutton, D. Environmental exposure to mercury and its toxicopathologic implications for public health. *Environmental Toxicology: An International Journal* **2003**, *18*, 149–175.
3. Flanders, J.R.; Long, G.; Reese, B.; Grosso, N.R.; Clements, W.; Stahl, R.G. Assessment of potential mercury toxicity to native invertebrates in a high-gradient stream. *Integrated Environmental Assessment and Management* **2019**, *15*, 374–384, doi:10.1002/ieam.4133.
4. Sall, M.L.; Fall, B.; Diédhiou, I.; Dièye, E.H.; Lo, M.; Diaw, A.K.D.; Gningue-Sall, D.; Raouafi, N.; Fall, M. Toxicity and Electrochemical Detection of Lead, Cadmium and Nitrite Ions by Organic Conducting Polymers: A Review. *Chemistry Africa* **2020**, doi:10.1007/s42250-020-00157-0.
5. Hande, P.E.; Samui, A.B.; Kulkarni, P.S. Selective nanomolar detection of mercury using coumarin based fluorescent Hg (II)—Ion imprinted polymer. *Sensors and Actuators B: Chemical* **2017**, *246*, 597–605.
6. Li, X.; Li, Z.; Wu, T.; Chen, J.; Fu, C.; Zhang, L.; Feng, X.; Fu, X.; Tang, L.; Wang, Z.; et al. Atmospheric mercury emissions from two pre-calciner cement plants in Southwest China. *Atmospheric Environment* **2019**, *199*, 177–188, doi:10.1016/j.atmosenv.2018.11.011.
7. Green, C.S.; Lewis, P.J.; Wozniak, J.R.; Drevnick, P.E.; Thies, M.L. A comparison of factors affecting the small-scale distribution of mercury from artisanal small-scale gold mining in a Zimbabwean stream system. *Science of The Total Environment* **2019**, *647*, 400–410, doi:10.1016/j.scitotenv.2018.07.418.
8. Balasundaram, K.; Sharma, M. Technology for mercury removal from flue gas of coal based thermal power plants: A comprehensive review. *Critical Reviews in Environmental Science and Technology* **2019**, *0*, 1–37, doi:10.1080/10643389.2019.1583050.
9. D'ltri, P.A.; D'ltri, F.M. Mercury contamination: a human tragedy. *Environmental Management* **1978**, *2*, 3–16.
10. Vijayaraghavan, K.; Yun, Y.-S. Bacterial biosorbents and biosorption. *Biotechnology advances* **2008**, *26*, 266–291.
11. Cariccio, V.L.; Samà, A.; Bramanti, P.; Mazzon, E. Mercury Involvement in Neuronal Damage and in Neurodegenerative Diseases. *Biol Trace Elem Res* **2019**, *187*, 341–356, doi:10.1007/s12011-018-1380-4.
12. Chen, G.; Guo, Z.; Zeng, G.; Tang, L. Fluorescent and colorimetric sensors for environmental mercury detection. *Analyst* **2015**, *140*, 5400–5443.
13. Fezai, F.; Gros, P.; Meireles, M.; Evrard, D. New Electrochemical Sensor for Hg(II) Trace Detection in Natural Waters: Electrode Functionalization with Gold Nanoparticles and Diazonium Salts. *Meet. Abstr.* **2019**, *MA2019-01*, 2010–2010.
14. Piletsky, S.A.; Turner, A.P.F. Electrochemical Sensors Based on Molecularly Imprinted Polymers. *Electroanalysis* **2002**, *14*, 317–323, doi:10.1002/1521-4109(200203)14:5<317::AID-ELAN317>3.0.CO;2-5.
15. Salmi, Z.; Benzarti, K.; Chehimi, M.M. Diazonium Cation-Exchanged Clay: An Efficient, Unfrequented Route for Making Clay/Polymer Nanocomposites. *Langmuir* **2013**, *29*, 13323–13328, doi:10.1021/la402710r.

16. Msaadi, R.; Ammar, S.; Chehimi, M.M.; Yagci, Y. Diazonium-based ion-imprinted polymer/clay nanocomposite for the selective extraction of lead (II) ions in aqueous media. *European Polymer Journal* **2017**, *89*, 367–380, doi:10.1016/j.eurpolymj.2017.02.029.
17. Lo, M.; Ktari, N.; Gningue-Sall, D.; Madani, A.; Aaron, S.E.; Aaron, J.-J.; Mekhalif, Z.; Delhalle, J.; Chehimi, M.M. Polypyrrole: a reactive and functional conductive polymer for the selective electrochemical detection of heavy metals in water. *Emergent Mater.* **2020**, doi:10.1007/s42247-020-00119-9.
18. Ktari, N.; Fourati, N.; Zerrouki, C.; Ruan, M.; Seydou, M.; Barbaut, F.; Nal, F.; Yaakoubi, N.; Chehimi, M.M.; Kalfat, R. Design of a polypyrrole MIP-SAW sensor for selective detection of flumequine in aqueous media. Correlation between experimental results and DFT calculations. *RSC Adv.* **2015**, *5*, 88666–88674, doi:10.1039/C5RA16237H.
19. Bahrami, A.; Besharati-Seidani, A.; Abbaspour, A.; Shamsipur, M. A highly selective voltammetric sensor for nanomolar detection of mercury ions using a carbon ionic liquid paste electrode impregnated with novel ion imprinted polymeric nanobeads. *Materials Science and Engineering: C* **2015**, *48*, 205–212, doi:10.1016/j.msec.2014.12.005.
20. Li, Z.-C.; Fan, H.-T.; Zhang, Y.; Chen, M.-X.; Yu, Z.-Y.; Cao, X.-Q.; Sun, T. Cd(II)-imprinted polymer sorbents prepared by combination of surface imprinting technique with hydrothermal assisted sol–gel process for selective removal of cadmium(II) from aqueous solution. *Chemical Engineering Journal* **2011**, *171*, 703–710, doi:10.1016/j.cej.2011.05.023.
21. Karrat, A.; Lamaoui, A.; Amine, A.; Palacios-Santander, J.M.; Cubillana-Aguilera, L. Applications of Chitosan in Molecularly and Ion Imprinted Polymers. *Chemistry Africa* **2020**, doi:10.1007/s42250-020-00177-w.
22. Fayazi, M.; Ghanei-Motlagh, M.; Taher, M.A.; Ghanei-Motlagh, R.; Salavati, M.R. Synthesis and application of a novel nanostructured ion-imprinted polymer for the preconcentration and determination of thallium(I) ions in water samples. *Journal of Hazardous Materials* **2016**, *309*, 27–36, doi:10.1016/j.jhazmat.2016.02.002.
23. Rajabi, H.R.; Razmpour, S. Synthesis, characterization and application of ion imprinted polymeric nanobeads for highly selective preconcentration and spectrophotometric determination of Ni2+ ion in water samples. *Spectrochimica Acta Part A: Molecular and Biomolecular Spectroscopy* **2016**, *153*, 45–52, doi:10.1016/j.saa.2015.08.010.
24. Ashkenani, H.; Taher, M.A. Use of ionic liquid in simultaneous microextraction procedure for determination of gold and silver by ETAAS. *Microchemical Journal* **2012**, *103*, 185–190, doi:10.1016/j.microc.2012.03.005.
25. Fu, J.; Chen, L.; Li, J.; Zhang, Z. Current status and challenges of ion imprinting. *J. Mater. Chem. A* **2015**, *3*, 13598–13627, doi:10.1039/C5TA02421H.
26. García-Otero,N.; Teijero-Valiño, C.; Otero-Romaní, J.; Peña-Vásquez, E.; Moreda-Piñeiro., A.; Bermejo-Barrera, P. On-line ionic imprinted polymer selective solid-phase extraction of nickel and lead from seawater and their determination by inductively coupled plasma-optical emission spectrometry. *Anal Bioanal Chem* **2009**, *395*, 1107–1115, doi:10.1007/s00216-009-3044-x.
27. Luo, X.; Liu, L.; Deng, F.; Luo, S. Novel ion-imprinted polymer using crown ether as a functional monomer for selective removal of Pb(II) ions in real environmental water samples. *J. Mater. Chem. A* **2013**, *1*, 8280–8286, doi:10.1039/C3TA11098B.

28. Gawin, M.; Konefał, J.; Trzewik, B.; Walas, S.; Tobiasz, A.; Mrowiec, H.; Witek, E. Preparation of a new Cd(II)-imprinted polymer and its application to determination of cadmium(II) via flow-injection-flame atomic absorption spectrometry. *Talanta* **2010**, *80*, 1305–1310, doi:10.1016/j.talanta.2009.09.021.
29. Abu-Dalo, M.A.; Al-Rawashdeh, N.A.F.; Al-Mheidat, I.R.; Nassory, N.S. Preparation and evaluation of new uranyl imprinted polymer electrode sensor for uranyl ion based on uranyl–carboxybezotriazole complex in pvc matrix membrane. *Sensors and Actuators B: Chemical* **2016**, *227*, 336–345, doi:10.1016/j.snb.2015.12.076.
30. Güney, S.; Güney, O. A novel electrochemical sensor for selective determination of uranyl ion based on imprinted polymer sol–gel modified carbon paste electrode. *Sensors and Actuators B: Chemical* **2016**, *231*, 45–53, doi:10.1016/j.snb.2016.02.119.
31. Alizadeh, T.; Ganjali, M.R.; Zare, M. Application of an Hg2+ selective imprinted polymer as a new modifying agent for the preparation of a novel highly selective and sensitive electrochemical sensor for the determination of ultratrace mercury ions. *Analytica Chimica Acta* **2011**, *689*, 52–59, doi:10.1016/j.aca.2011.01.036.
32. Rajabi, H.R.; Roushani, M.; Shamsipur, M. Development of a highly selective voltammetric sensor for nanomolar detection of mercury ions using glassy carbon electrode modified with a novel ion imprinted polymeric nanobeads and multi-wall carbon nanotubes. *Journal of Electroanalytical Chemistry* **2013**, *693*, 16–22, doi:10.1016/j.jelechem.2013.01.003.
33. Fu, X.-C.; Wu, J.; Nie, L.; Xie, C.-G.; Liu, J.-H.; Huang, X.-J. Electropolymerized surface ion imprinting films on a gold nanoparticles/single-wall carbon nanotube nanohybrids modified glassy carbon electrode for electrochemical detection of trace mercury(II) in water. *Analytica Chimica Acta* **2012**, *720*, 29–37, doi:10.1016/j.aca.2011.12.071.
34. Fu, X.-C.; Chen, X.; Guo, Z.; Xie, C.-G.; Kong, L.-T.; Liu, J.-H.; Huang, X.-J. Stripping voltammetric detection of mercury(II) based on a surface ion imprinting strategy in electropolymerized microporous poly(2-mercaptobenzothiazole) films modified glassy carbon electrode. *Analytica Chimica Acta* **2011**, *685*, 21–28, doi:10.1016/j.aca.2010.11.020.
35. Li, M.; Gou, H.; Al-Ogaidi, I.; Wu, N. Nanostructured Sensors for Detection of Heavy Metals: A Review. *ACS Sustainable Chem. Eng.* **2013**, *1*, 713–723, doi:10.1021/sc400019a.
36. Litton, C.W.; Collins, T.C.; Reynolds, D.C. *Zinc Oxide Materials for Electronic and Optoelectronic Device Applications*; John Wiley & Sons, 2011; ISBN 978-1-119-99121-2.
37. Özgür, Ü.; Alivov, Ya.I.; Liu, C.; Teke, A.; Reshchikov, M.A.; Doğan, S.; Avrutin, V.; Cho, S.-J.; Morkoç, H. A comprehensive review of ZnO materials and devices. *Journal of Applied Physics* **2005**, *98*, 041301, doi:10.1063/1.1992666.
38. Nandi, R.; Major, S.S. The mechanism of growth of ZnO nanorods by reactive sputtering. *Applied Surface Science* **2017**, *399*, 305–312, doi:10.1016/j.apsusc.2016.12.097.
39. Mekki, A.; Ait-Touchente, Z.; Samanta, S.; Singh, A.; Mahmoud, R.; Chehimi, M.M.; Aswal, D.K. Polyaniline-Wrapped ZnO Nanorod Composite Films on Diazonium-Modified Flexible Plastic Substrates. *Macromolecular Chemistry and Physics* **2016**, *217*, 1136–1148, doi:10.1002/macp.201500430.
40. Pacholski, C.; Kornowski, A.; Weller, H. Self-Assembly of ZnO: From Nanodots to Nanorods. *Angewandte Chemie International Edition* **2002**, *41*, 1188–1191, doi:10.1002/1521-3773(20020402)41:7<1188::AID-ANIE1188>3.0.CO;2-5.

41. Chander, R.; Raychaudhuri, A.K. Growth of aligned arrays of ZnO nanorods by low temperature solution method on Si surface. *J Mater Sci* **2006**, *41*, 3623–3630, doi:10.1007/s10853-006-6218-3.
42. Ait-Touchente, Z.; Sakhraoui, H.E.E.Y.; Fourati, N.; Zerrouki, C.; Maouche, N.; Touzani, R.; Yaakoubi, N.; Chehimi, M.M. Zinc Oxide Nanorods Wrapped with Ion-Imprinted Polypyrrole Polymer for Picomolar Selective and Electrochemical Detection of Mercury II Ions. *Proceedings* **2018**, *2*, 1004, doi:10.3390/proceedings2131004.
43. Lo, M.; Pires, R.; Diaw, K.; Gningue-Sall, D.; Oturan, M.A.; Aaron, J.-J.; Chehimi, M.M. Diazonium salts: versatile molecular glues for sticking conductive polymers to flexible electrodes. *Surfaces* **2018**, *1*, 43–58.
44. Adenier, A.; Bernard, M.-C.; Chehimi, M.M.; Cabet-Deliry, E.; Desbat, B.; Fagebaume, O.; Pinson, J.; Podvorica, F. Covalent Modification of Iron Surfaces by Electrochemical Reduction of Aryldiazonium Salts. *J. Am. Chem. Soc.* **2001**, *123*, 4541–4549, doi:10.1021/ja003276f.
45. Claude, B. Intérêt des polymères à empreintes moléculaires pour la préparation d'échantillons par extraction solide-liquide. *Applications Aux Triterpènes Dans Les Plantes et Aux Dopants Dans Les Urines., Université d'Orléans* **2007**.
46. Watson, C.M.; Dwyer, D.J.; Andle, J.C.; Bruce, A.E.; Bruce, M.R.M. Stripping Analyses of Mercury Using Gold Electrodes: Irreversible Adsorption of Mercury. *Anal. Chem.* **1999**, *71*, 3181–3186, doi:10.1021/ac981312b.
47. Ordeig, O.; Banks, C.E.; del Campo, J.; Muñoz, F.X.; Compton, R.G. Trace Detection of Mercury(II) Using Gold Ultra-Microelectrode Arrays. *Electroanalysis* **2006**, *18*, 573–578, doi:10.1002/elan.200503437.
48. Vasjari, M.; Shirshov, Y.M.; Samoylov, A.V.; Mirsky, V.M. SPR investigation of mercury reduction and oxidation on thin gold electrodes. *Journal of Electroanalytical Chemistry* **2007**, *605*, 73–76, doi:10.1016/j.jelechem.2007.03.019.
49. Manceau, A.; L. Nagy, K. Relationships between Hg(ii)–S bond distance and Hg(ii) coordination in thiolates. *Dalton Transactions* **2008**, *0*, 1421–1425, doi:10.1039/B718372K.
50. Berthon, G. Critical evaluation of the stability constants of metal complexes of amino acids with polar side chains (Technical Report). *Pure and Applied Chemistry* **1995**, *67*, 1117–1240, doi:10.1351/pac199567071117.
51. Sakhraoui, H.E.E.Y.; Mazouz, Z.; Attia, G.; Fourati, N.; Zerrouki, C.; Maouche, N.; Othmane, A.; Yaakoubi, N.; Kalfat, R.; Madani, A.; et al. Design of L-Cysteine and Acrylic Acid Imprinted Polypyrrole Sensors for Picomolar Detection of Lead Ions in Simple and Real Media. *IEEE Sensors Journal* **2019**, 1–1, doi:10.1109/JSEN.2019.2961984.
52. Ding, N.; Zhao, H.; Peng, W.; He, Y.; Zhou, Y.; Yuan, L.; Zhang, Y. A simple colorimetric sensor based on anti-aggregation of gold nanoparticles for Hg2+ detection. *Colloids and Surfaces A: Physicochemical and Engineering Aspects* **2012**, *395*, 161–167, doi:10.1016/j.colsurfa.2011.12.024.
53. Mah, V.; Jalilehvand, F. Mercury (II) complex formation with glutathione in alkaline aqueous solution. *JBIC Journal of Biological Inorganic Chemistry* **2008**, *13*, 541–553.
54. Ballav, N.; Das, R.; Giri, S.; Muliwa, A.M.; Pillay, K.; Maity, A. L-cysteine doped polypyrrole (PPy@ L-Cyst): a super adsorbent for the rapid removal of Hg+ 2 and efficient catalytic activity of the spent adsorbent for reuse. *Chemical Engineering Journal* **2018**, *345*, 621–630.

55. Mazouz, Z.; Touchente, Z.A.; Laradi, H.; Fourati, N.; Yaakoubi, N.; Touzani, R.; Chehimi, M.M.; Kalfat, R.; Othmane, A.; Zerrouki, C. Design of Novel Electrochemical Sensors for the Selective Detection of Glyphosate. In Proceedings of the Multidisciplinary Digital Publishing Institute Proceedings; 2017; Vol. 1, p. 483.
56. Teng, Z.; Lv, H.; Wang, L.; Liu, L.; Wang, C.; Wang, G. Voltammetric Sensor Modified by EDTA-immobilized Graphene-like Carbon Nitride Nanosheets: Preparation, Characterization and Selective Determination of Ultra-Trace Pb (II) in Water Samples. *Electrochimica Acta* **2016**, *212*, 722–733, doi:10.1016/j.electacta.2016.07.036.
57. Repo, E.; Malinen, L.; Koivula, R.; Harjula, R.; Sillanpää, M. Capture of Co(II) from its aqueous EDTA-chelate by DTPA-modified silica gel and chitosan. *Journal of Hazardous Materials* **2011**, *187*, 122–132, doi:10.1016/j.jhazmat.2010.12.113.
58. Hinck, M.L.; Ferguson, J.; Puhaakka, J. Resistance of EDTA and DTPA to aerobic biodegradation. *Water Science and Technology* **1997**, *35*, 25–31, doi:10.1016/S0273-1223(96)00911-0.
59. Mazouz, Z.; Rahali, S.; Fourati, N.; Zerrouki, C.; Aloui, N.; Seydou, M.; Yaakoubi, N.; Chehimi, M.M.; Othmane, A.; Kalfat, R. Highly Selective Polypyrrole MIP-Based Gravimetric and Electrochemical Sensors for Picomolar Detection of Glyphosate. *Sensors* **2017**, *17*, 2586, doi:10.3390/s17112586.
60. Roushani, M.; Saedi, Z.; Hamdi, F.; Dizajdizi, B.Z. Preparation an electrochemical sensor for detection of manganese (II) ions using glassy carbon electrode modified with multi walled carbon nanotube-chitosan-ionic liquid nanocomposite decorated with ion imprinted polymer. *Journal of Electroanalytical Chemistry* **2017**, *804*, 1–6.
61. Alizadeh, T.; Rafiei, F.; Hamidi, N.; Ganjali, M.R. A new electrochemical sensing platform for Cr (III) determination based on nano-structured Cr (III)-imprinted polymer-modified carbon composite electrode. *Electrochimica Acta* **2017**, *247*, 812–819.
62. Alizadeh, T.; Hamidi, N.; Ganjali, M.R.; Rafiei, F. An extraordinarily sensitive voltammetric sensor with picomolar detection limit for Pb2+ determination based on carbon paste electrode impregnated with nano-sized imprinted polymer and multi-walled carbon nanotubes. *Journal of environmental chemical engineering* **2017**, *5*, 4327–4336.
63. Karthika, A.; Ramasamy Raja, V.; Karuppasamy, P.; Suganthi, A.; Rajarajan, M. Electrochemical behaviour and voltammetric determination of mercury (II) ion in cupric oxide/poly vinyl alcohol nanocomposite modified glassy carbon electrode. *Microchemical Journal* **2019**, *145*, 737–744, doi:10.1016/j.microc.2018.11.030.
64. Shirzadmehr, A.; Afkhami, A.; Madrakian, T. A new nano-composite potentiometric sensor containing an Hg2+-ion imprinted polymer for the trace determination of mercury ions in different matrices. *Journal of Molecular Liquids* **2015**, *204*, 227–235, doi:10.1016/j.molliq.2015.01.014.
65. Armas, M.A.; María-Hormigos, R.; Cantalapiedra, A.; Gismera, M.J.; Sevilla, M.T.; Procopio, J.R. Multiparametric optimization of a new high-sensitive and disposable mercury (II) electrochemical sensor. *Analytica Chimica Acta* **2016**, *904*, 76–82, doi:10.1016/j.aca.2015.11.016.
66. Shah, A.; Sultan, S.; Zahid, A.; Aftab, S.; Nisar, J.; Nayab, S.; Qureshi, R.; Khan, G.S.; Hussain, H.; Ozkan, S.A. Highly sensitive and selective electrochemical sensor for the trace level detection of mercury and cadmium. *Electrochimica Acta* **2017**, *258*, 1397–1403, doi:10.1016/j.electacta.2017.12.002.

67. Ganjali, M.R.; Rahmani, A.R.; Shokoohi, R.; Farmany, A.; Khazaei, M. A Highly Sensitive and Selective Electrochemical Mercury (II) Sensor Based on Nanoparticles of Hg (II)-imprinted Polymer and Graphitic Carbon Nitride (gC 3N4). *Int. J. Electrochem. Sci* **2019**, *14*, 6420–6430.
68. Devi, N.R.; Sasidharan, M.; Sundramoorthy, A.K. Gold Nanoparticles-Thiol-Functionalized Reduced Graphene Oxide Coated Electrochemical Sensor System for Selective Detection of Mercury Ion. *J. Electrochem. Soc.* **2018**, *165*, B3046–B3053, doi:10.1149/2.0081808jes.
69. Sánchez-Calvo, A.; Fernández-Abedul, M.T.; Blanco-López, M.C.; Costa-García, A. Paper-based electrochemical transducer modified with nanomaterials for mercury determination in environmental waters. *Sensors and Actuators B: Chemical* **2019**, *290*, 87–92, doi:10.1016/j.snb.2019.03.089.